IEEE Access
Multidisciplinary : Rapid Review : Open Access Journal

Received 7 April 2026, accepted 8 May 2026, date of publication 15 May 2026, date of current version 26 May 2026.
Digital Object Identifier 10.1109/ACCESS.2026.3693983

RESEARCH ARTICLE

Near-Field LoS MIMO Channel Representation Based on Consecutively Pairwise-Division for Phase Linearization

WOONG-HEE LEE[1], (Member, IEEE), DONG-HWAN KIM[1], HYUNDUK KANG[2], HO-KYUNG SON[2], JONG-HO LEE[3], (Member, IEEE), AND NAMYOON LEE[4], (Senior Member, IEEE)
[1]Division of Electronics and Electrical Engineering, Dongguk University-Seoul Campus, Seoul 04620, South Korea
[2]Radio Technology Research Section, Electronics and Telecommunications Research Institute, Daejeon 34129, South Korea
[3]School of Electronic Engineering, Soongsil University, Seoul 06978, South Korea
[4]Department of Electrical Engineering, POSTECH, Pohang 37673, South Korea

Corresponding author: Namyoon Lee (nylee@postech.ac.kr)

This work was supported in part by the Institute of Information and Communications Technology Planning and Evaluation (IITP) grant funded by Korean Government (MSIT), Development of Integrated Interference Analysis Technology for Improving Frequency Utilization Efficiency under Grant RS-2023-00217885; and in part by the Dongguk University Research Fund of 2024 under Grant S-2024-G0001-00025.

ABSTRACT In this paper, we propose a new channel representation method that facilitates a user localization problem in near-field line-of-sight (LoS) channel environments. Our approach is to harness a phase linearization method. Unlike a far-field channel model, the phase response of the near-field channel is characterized as a quadratic function across antennas, which arises from the second-order Taylor approximation of the spherical wavefront. Thus, in a continuous domain, the differentiation of this function yields a linear function, which forms the basis of our method. To implement this in the spatial sampling domain, pairwise division relationships are established between the elements of the observed channel. We refer to this near-field LoS MIMO channel representation based on consecutively pairwise division (CPD). More specifically, there are two representative types of patterns in terms of the index pairing pattern. One pattern maintains a constant difference between indices, whereas the other maintains a constant sum. In order to validate our proposed CPD method, we demonstrate through simulations that our approach enables user localization with significantly improved accuracy compared to conventional methods.

INDEX TERMS Pairwise-division, near-field, line-of-sight, phase linearization, user localization.

I. INTRODUCTION

The advent of sixth-generation (6G) wireless networks marks a significant leap forward in communication technologies, offering unprecedented data rates, ultra-low latency, and extensive connectivity. For instance, extended reality (XR), digital twins, Metaverse, and autonomous transportation systems require high-level technologies for 6G networks. A cornerstone of 6G is the integration of extremely large-scale multiple-input multiple-output (XL-MIMO) systems [1], which leverage a massive number of antennas to substantially improve spatial degrees of freedom and spectral efficiency [2]. Unlike conventional massive MIMO, XL-MIMO can simultaneously serve a large number of users and create highly focused beams. These systems often employ extremely large aperture arrays (ELAA), designed to operate primarily in the radiative near-field region. This near-field environment introduces distinctive electromagnetic (EM) phenomena that fundamentally differ from conventional far-field propagation, creating both challenges and opportunities for advancing wireless communication technologies. Effectively understanding and harnessing these near-field characteristics is crucial for optimizing next-generation communication systems and unlocking the full potential of 6G [3], [4].

In near-field XL-MIMO systems, the EM waves radiated from the antenna array exhibit spherical wavefronts, in contrast to the plane wave approximation typically

The associate editor coordinating the review of this manuscript and approving it for publication was Bilal A. Khawaja.

assumed in far-field conditions. The boundary between the far-field and near-field is characterized by the Fraunhofer distance (also known as the Rayleigh distance), which represents the minimum propagation distance at which the phase difference across array elements remains within 22.5 degrees [5]. Conventional massive MIMO systems have a relatively smaller number of antennas than XL-MIMO systems; therefore, the Rayleigh distance is negligible. Therefore, most of conventional communication algorithms were primarily developed with far-field-based theories and techniques [6]. However, as the number of antennas continues to grow dramatically in XL-MIMO systems, the Rayleigh distance expands significantly, thereby expanding the near-field region [7], which demonstrates that one cannot use conventional far-field-based algorithms effectively. More importantly, this implies that near-field effects are no longer confined to short-range communications, but can emerge even for users located at several hundred meters from the base station, particularly at millimeter-wave and terahertz frequencies where the wavelength is extremely small. Consequently, the expanded near-field region introduces both new opportunities, such as ultra-precise beam focusing, user localization and new challenges in terms of channel modeling and algorithm design.

This spherical nature introduces a more complex modeling approach that considers variations in both angle and distance across the array elements. Unlike the far-field scenario, where angles of arrival and departure are assumed constant across the array, near-field propagation demands precise phase and amplitude adjustments to accurately capture the channel characteristics. Notwithstanding its complex channel representation, the spherical wavefronts provide a richer set of spatial information, enabling highly accurate beamforming (or beam-focusing [8], [9], [10]) and enhanced user localization capabilities [11], [12], [13]. Moreover, since the near-field beam-focusing effect can be exploited to mitigate inter-functionality interference, it is suitable for integrated sensing and communication (ISAC) systems [14]. This fundamental transition from plane waves to spherical waves represents a critical enabler for the advanced functionalities envisioned in 6G networks. Therefore, understanding and addressing the modeling challenges and practical implications of spherical wave propagation are pivotal for the successful deployment of near-field XL-MIMO systems.

The near-field localization problem is closely linked to the near-field line-of-sight (LoS) channel representation, as it is fully determined by the relative position of a user to the base station. Moreover, previous works [15], [16], [17] have shown that the LoS channel is dominant in short-range MIMO systems, further emphasizing the importance of accurate LoS channel modeling for localization. Several methods have been proposed to represent the near-field LoS channel, which facilitate the user localization problem [4], [18], [19], [20], [21], [22]. Specifically, the polar-domain method [18], [19] provides mathematically useful information of the near-field channel by jointly considering angle and distance information, thereby constructing an efficient dictionary for channel estimation and user localization. Moreover, this representation is used to ensure the sparsity of the near-field channel, enabling the utilization of compressive sensing methods, e.g., orthogonal matching pursuit (OMP) and simultaneous iterative gridless weighted (SIGW) algorithms [18]. However, its high computational complexity grows with the number of antennas, limiting the practical implementation. Moreover, sub-array configurations [20], [21], [22] in XL-MIMO systems attempt to reduce the complexity by dividing the antenna array into smaller partitions, which makes the processing more tractable and scalable. Nevertheless, this simplification fundamentally limits the spatial resolution, since partitioning the array reduces the effective aperture and interrupts the achievable localization accuracy.

To overcome these limitations, in this paper, we introduce a novel near-field channel representation method that offers high spatial resolution and low-computational complexity to estimate the quadratic phase function. The key idea of our method is to harness the linearity in the fraction across the phase response.

The main contributions are three-fold as follows:

- We introduce a novel near-field LoS channel representation method based on consecutively pairwise-division (CPD), which is specifically designed to achieve phase linearization. This approach not only enhances the accuracy of channel representations in complex near-field scenarios but also provides a more robust framework for signal processing in challenging environments.
- The proposed method demonstrates notable versatility by creating new channel representations through element-wise division according to specific index patterns. In this paper, we highlight two primary approaches: first, by sliding element pairs with a predefined spacing, and second, by symmetrically selecting element pairs as the indices move outward from the central element. These are only two examples of the many possible patterns that can be used, especially considering the wide range of phase-linearizable extraction schemes.
- Using the CPD approach, we propose a new method for near-field user localization based on precise parameter estimation. Our approach is characterized by its computational simplicity, making it both efficient and scalable. Additionally, the proposed method shows a strong potential for adaptation to various objectives such as beam-focusing, which suggest its applicability across a wide range of scenarios and system architectures in near-field systems.

The remainder of this paper is organized as follows: Section II introduces the system model in near-field environment. In Section III, we presents our proposed method with applications and few remarks. In Section IV, we provide numerical results to demonstrate the robustness

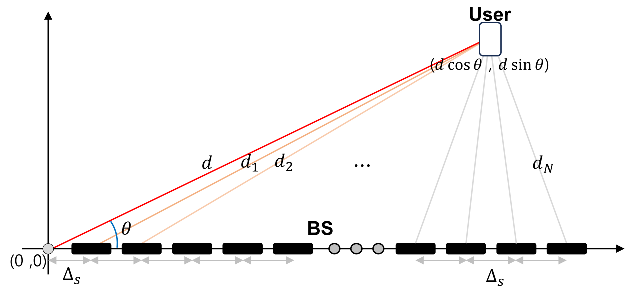

FIGURE 1. **Illustration of the system model.**

and superiority of proposed method in the aspects of various environments. Finally, Section V presents the concluding remarks.

II. SYSTEM MODEL

We consider an uplink scenario where a BS equipped with an ELAA—implemented as a uniform linear array (ULA) with N isotropic antennas—communicates with a user having a single isotropic antenna. Here, the coordinates of a single antenna user are given by $(d\cos\theta, d\sin\theta)$, where d and θ are the distance and angle, respectively, between the BS and the user. Without loss of generality, the BS antenna array is aligned along the x-axis with the inter-antenna spacing Δ_s. Readers can understand system model including the ULA more easily through Fig. 1.

In a free-space propagation scenario, the channel response between the n-th antenna in the ULA and a user can be expressed as follows:

$$h_n = \sqrt{\beta_n} e^{-j\frac{2\pi}{\lambda} d_n}, \tag{1}$$

where d_n is the distance between the n-th antenna in the ULA and a user. More specifically, this can be formulated as follows:

$$d_n = d\sqrt{1 + \frac{(n\Delta_s)^2}{d^2} - \frac{2n\Delta_s}{d}\cos\theta}. \tag{2}$$

In addition, the channel gain is approximately constant among the antennas so that $\beta_n = \beta = \frac{\lambda^2}{(4\pi d)^2}, \forall n$ [23]. Consider N-sized channel $\mathbf{h}$, then it can be represented as follows:

$$\mathbf{h} = [h_1, h_2, \cdots, h_N]^{\mathrm{T}} = h_c \mathbf{b}(\theta, d), \tag{3}$$

where $\mathbf{b}(\theta, d) = [e^{-j\frac{2\pi(d_1-d)}{\lambda}}, \cdots, e^{-j\frac{2\pi(d_N-d)}{\lambda}}]^{\mathrm{T}}$ is the near-field array response vector and $h_c \triangleq \sqrt{\beta} e^{-j\frac{2\pi d}{\lambda}}$.

III. CONSECUTIVE PAIRWISE-DIVISION-BASED PHASE LINEARIZATION METHODS

In this section, we introduce consecutively pairwise-division approaches to represent the near-field LoS MIMO channel. Using the second-order Taylor approximation [24], $\sqrt{1+x} \simeq 1 + \frac{1}{2}x - \frac{1}{8}x^2$, the phase of the n-th antenna defined in (2) is approximated as

$$\begin{aligned} d_n &= d\sqrt{1 + \frac{(n\Delta_s)^2}{d^2} - \frac{2n\Delta_s}{d}\cos\theta} \\ &\simeq d\Bigg(1 + \frac{1}{2}\Big(\frac{(n\Delta_s)^2}{d^2} - \frac{2n\Delta_s}{d}\cos\theta\Big) \\ &\quad - \frac{1}{8}\Big(\frac{(n\Delta_s)^2}{d^2} - \frac{2n\Delta_s}{d}\cos\theta\Big)^2\Bigg) \\ &\simeq d - n\Delta_s\cos\theta + \frac{(n\Delta_s)^2}{2d}\sin^2\theta \end{aligned} \tag{4}$$

where the final expression follows from the second-order Taylor approximation, commonly referred to as the Fresnel approximation.

This phase response is quadratic in $n\Delta_s$. We let $n\Delta_s = u$ be a continuous value on $\mathbb{R}$, i.e., assuming that $n \in \mathbb{Z}$ and Δ_s goes to 0. Then, the continuous quadratic phase response function is defined on $\mathbb{R}$ as

$$d_n(u) \simeq d - u\cos\theta + \frac{\sin^2\theta}{2d}u^2. \tag{5}$$

By taking the derivative with respect to u, we have a linear function in u as

$$\frac{\partial d_n(u)}{\partial u} \simeq -\cos\theta + \frac{\sin^2\theta}{d}u. \tag{6}$$

This phase linearization by the differential operator facilitates estimating physical parameters in the near-field LoS channel. However, due to the spatially discrete nature of the channels, the derivative is not feasible. This problem is addressed by introducing two methods based on index-difference patterns, detailed in the following subsections.

A. PROPOSED CPD CHANNEL REPRESENTATION #1

Treating m as the index spacing, we consider all corresponding pairs (h_n, h_{n+m}) across all n. This representation ensures the constant difference, i.e., m, between indices for all n. Naturally,

$$h_{n+m} = \sqrt{\beta} e^{-j\frac{2\pi}{\lambda} d_{n+m}}, \tag{7}$$

where $d_{n+m} \simeq d - (n+m)\Delta_s\cos\theta + \big(\frac{(n+m)^2\Delta_s^2\sin^2\theta}{2d}\big)$. Now, we can define the CPD channel #1, denoted by $\mathbf{q}(\mathbf{h}; m) = [q_1, \cdots, q_{N-m}]^{\mathrm{T}}$, as follows for all $n \in \{1, \cdots, N-m\}$:

$$q_n \triangleq \frac{h_{n+m}}{h_n} = e^{-j\frac{2\pi}{\lambda}(d_{n+m}-d_n)}. \tag{8}$$

Next, let us expand the term $d_{n+m} - d_n$ as follows:

$$\begin{aligned} d_{n+m} - d_n &\simeq -m\Delta_s\cos\theta + (2nm + m^2)\Delta_s^2\big(\frac{\sin^2\theta}{2d}\big) \\ &= \big(\frac{m\Delta_s^2\sin^2\theta}{d}\big)n + \frac{m}{2}\big(\frac{m\Delta_s^2\sin^2\theta}{d} - 2\Delta_s\cos\theta\big). \end{aligned} \tag{9}$$

Consequently, $\mathbf{q}(\mathbf{h}; m)$ is modeled as a linear phase with respect to the drifting index n. Here, the term $\frac{\Delta_s^2\sin^2\theta}{d}$ plays a key role in determining the spatial frequency of the model and will reappear in the next channel modeling method.

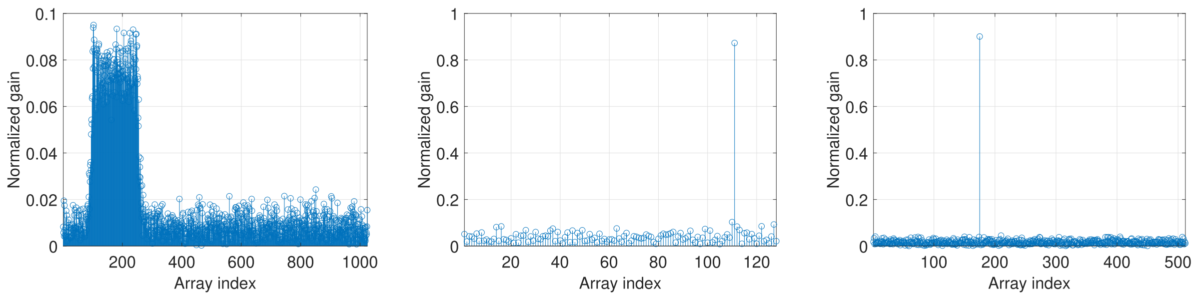

(a) Original channel (size: 1024) (b) CPD channel #1 (size: 128) (c) CPD channel #2 (size: 512)

FIGURE 2. **Array response in angular domain ($d = 15$ meters, $\theta = \pi/3$ radian, SNR = 10 dB, $\lambda = 0.0125$ meters, and $N = 1024$).**

B. PROPOSED CPD CHANNEL REPRESENTATION #2

Similarly to the previous subsection, we newly define the index pattern to maintain the summation of indices constant. Therefore, we can additionally define the CPD channel #2, denoted by $\mathbf{p}(\mathbf{h}) = [p_1, \cdots, p_{N/2}]^{\mathrm{T}}$, as follows for all $k \in \{1, \cdots, N/2\}$:

$$p_k \triangleq \frac{h_{N/2+k}}{h_{N/2-k+1}} = e^{-j\frac{2\pi}{\lambda}(d_{N/2+k}-d_{N/2-k+1})}. \tag{10}$$

Here, the term $d_{N/2+k} - d_{N/2-k+1}$ can be approximated as

$$d_{N/2+k} - d_{N/2-k+1} \simeq \big((N+1)(\frac{\Delta_s^2 \sin^2\theta}{d}) - 2\Delta_s \cos\theta\big)k. \tag{11}$$

As in the previous subsection, $\mathbf{p}(\mathbf{h})$ exhibits a linear phase characteristic. Furthermore, the term $\frac{\Delta_s^2 \sin^2\theta}{d}$ is included in both (9) and (11), playing a crucial role in the proposed channel modeling and parameter estimation with regard to the spatial frequency.

C. CHANNEL PARAMETER ESTIMATION FOR USER LOCALIZATION

In this subsection, we focus on near-field user localization through uplink transmissions. The objective is to estimate the angle, θ, and the distance, d, between the BS and the user. Using a ULA at the BS, the received signal depends on both θ and d, and our goal is to accurately extract these parameters from the uplink channel measurements.

Based on CPD channel #1, $\mathbf{q}(\mathbf{h}; m)$, and CPD channel #2, $\mathbf{p}(\mathbf{h})$ we will estimate the location of the user, θ and d. The term $\frac{\Delta_s^2 \sin^2\theta}{d}$ appears in both (9) and (11), and it can be regarded as the most essential term in our proposed method. For simplicity, let us denote the term $\frac{\Delta_s^2 \sin^2\theta}{d}$ as ψ. Then, CPD channel #1, $\mathbf{q}(\mathbf{h}; m)$, can be reformulated as follows for all n:

$$q_n \simeq e^{-j\frac{2\pi}{\lambda}\frac{m}{2}(m\psi - 2\Delta_s\cos\theta)} \cdot e^{-j\frac{2\pi}{\lambda}(m\psi)n}, \tag{12}$$

where $m\psi$ is the spatial frequency of $\mathbf{q}$. Similarly, CPD channel #2, $\mathbf{p}(\mathbf{h})$, can be reformulated as follows for all k:

$$p_k \simeq e^{-j\frac{2\pi}{\lambda}((N+1)\psi - 2\Delta_s\cos\theta)k}, \tag{13}$$

where $(N+1)\psi - 2\Delta_s\cos\theta$ is the spatial frequency of $\mathbf{p}$.

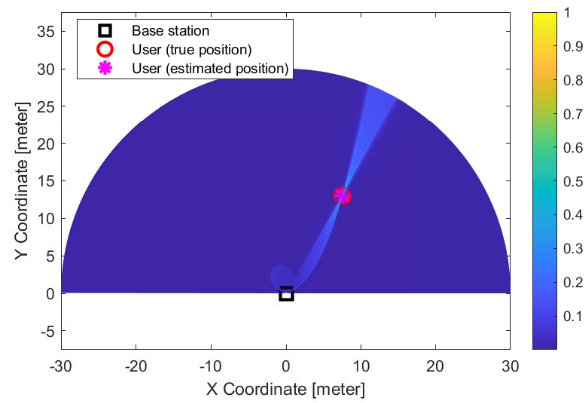

FIGURE 3. **A one-shot example of beam-focusing based on the proposed method (The parameter setting is equal to Fig. 2).**

Our approach enables reliable estimation of spatial frequencies $m\psi$ and $(N+1)\psi - 2\Delta_s\cos\theta$, associated with the phase components $\mathbf{q}$ and $\mathbf{p}$, respectively. Spatial frequency estimation yields $\psi(= \frac{\Delta_s^2 \sin^2\theta}{d})$, which in turn enables the retrieval of the underlying parameters θ and d. Overall, Algorithm 1 provides a summary of the proposed method.

D. AN EXAMPLE OF USER LOCALIZATION AND BEAM-FOCUSING

Fig. 2 shows the phase linearization of the the near-field channel. Fig. 2a illustrates the array response obtained through discrete Fourier transform (DFT) processing of the near-field channel in the angular domain. Due to the non-linear phase, it is not possible to identify the meaningful peak, which prevents the estimation of essential channel information such as angle and distance. In contrast, as shown in Figs 2b and 2c, the proposed CPD method enables the estimation of the channel parameters. Additionally, Fig. 3 illustrates beam-focusing under the same parameter settings as those presented in Fig. 2. The analysis of near-field channels demonstrates that beam-focusing can be achieved in a manner analogous to beamforming in the far-field. This approach involves pre-processing techniques that concentrate energy at specific points, rather than merely controlling the directionality of the beam. In near-field scenarios, beam-focusing—whose effectiveness critically depends on accurate user location—becomes more robust when applied with the proposed approach.

E. ANALYSIS OF LINEARIZATION QUALITY

Fig. 4 shows the phase characteristics of the near-field channel. Fig. 4a illustrates the unwrapped phase of the original channel, exhibiting the non-linear phase with respect to the array index due to the spherical wavefront in the near-field environment. In contrast, as shown in Figs 4b and 4c, the proposed CPD channels (CPD channel #1 and CPD channel #2) illustrate the approximately linear phase characteristic. This result explains that the CPD channels effectively eliminate the non-linearity of the near-field channel; thereby, one can directly use existing far-field-based algorithms without significant performance loss.

Fig. 5 shows the normalized mean squared error (NMSE) of the second-order Taylor approximation of the near-field channel with respect to angle θ and distance d. As shown in the figure, the original channel is compared with CPD channels demonstrating that the approximation error consistently remains at a low level and exhibits almost identical patterns across different channel sizes. Moreover, the approximation error tends to be minimized around the physical angles 0 and π, with decreases again near $\pi/2$. These results demonstrate that the approximation error is determined dominantly by angle θ rather than by the distance d.

F. REMARKS ON THE PROPOSED METHOD

1) VERSATILITIES IN TERMS OF INDEX SELECTION RULES

Our method offers considerable versatility by generating new channel representations through element-wise division based on specific index patterns. We focus on two key approaches: first, by sliding over the element pairs with a predetermined spacing between indices, and second, by symmetrically pairing elements as the indices move away from the center. These are just two of many potential patterns that can be employed, particularly when considering the range of phase-linearizable extraction schemes. The flexibility of this approach allows for multiple configurations, each of which could yield different insights. Specifically, the shifting index m in the proposed CPD channel #1 is an important parameter for extracting the core information ψ. Fig. 6 illustrates the estimation error of ψ with respect to the size of CPD channel #1, where the size is given by $N - m$. As shown in the figure, the estimation error exhibits a curved (U-shaped) behavior with respect to m. When m is too small, the effective phase slope $m\psi$ becomes small, making spatial-frequency estimation less robust to noise. On the other hand, when m is too large, the effective channel size $N-m$ decreases, reducing the number of usable samples and increasing the estimation variance. Therefore, there exists an optimal intermediate value of m that balances frequency resolution and statistical reliability.

Algorithm 1 CPD-Based User Localization

1: [*CPD-based representation phase*].
2: Measure N-sized original channel $\mathbf{h}$ and determine index spacing m.
3: Design $(N - m)$-sized CPD channel #1, i.e., $\mathbf{q}(\mathbf{h}; m)$, based on (8).
4: Design $N/2$-sized CPD channel #2, i.e., $\mathbf{p}(\mathbf{h})$, based on (10).
5: [*User localization phase*].
6: Extract the core information $\psi\left(\triangleq \frac{\Delta_s^2 \sin^2\theta}{d}\right)$ through a proper spatial frequency estimation method, e.g., a DFT process for $\mathbf{q}(\mathbf{h}; m)$ and $\mathbf{p}(\mathbf{h})$.
7: Estimate θ and d by combining the obtained ψ and the result of spatial frequency estimation for $\mathbf{p}(\mathbf{h})$.

2) COMPUTATIONAL COMPLEXITY

Our approach significantly reduces the computational complexity of near-field channel analysis and user localization by representing the array of size N into two smaller arrays: one of size $N - m$ and the other of size $N/2$. For each channel representation, we apply fast Fourier transform (FFT) operations, avoiding the higher complexity of traditional methods such as matching pursuit. The overall complexity is simplified to $O(N' \log N')$ where $N' = \max(N - m, N/2)$, representing a substantial reduction in computational cost.

3) SNR DEGRADATION

Our method introduces the pairwise-division operation in the near-field channel analysis, which inherently results in the signal-to-noise ratio (SNR) reduction. Specifically, the SNR observed across the combined channel elements is lower than the SNR experienced by the original N-sized array. This is due to our technique involving element-wise division, which leads to a reduction in the effective SNR. Notwithstanding this SNR loss, i.e., almost -3 dB, by applying appropriate denoising techniques, the performance can be further improved, making this method even more effective in practical scenarios.

4) MIXED LoS AND NLoS PROPAGATION

Channel estimation in the near-field differs fundamentally from that in the far-field, as it involves simultaneously extracting both distance and angle information. Naturally, this process aligns with the user localization. However, significant challenges emerge when both LoS and NLoS components are present, as multipath propagation complicates accurate estimation. Furthermore, our proposed CPD method achieves superior results when the numerator and denominator of the pairwise-division operation each contain only a single term (i.e.,as the K-factor approaches infinity), which is consistent with the principles of traditional user localization. Therefore, further exploration to extend the CPD method to provide closed-form solutions even in the presence of NLoS components or additive noise would be highly beneficial.

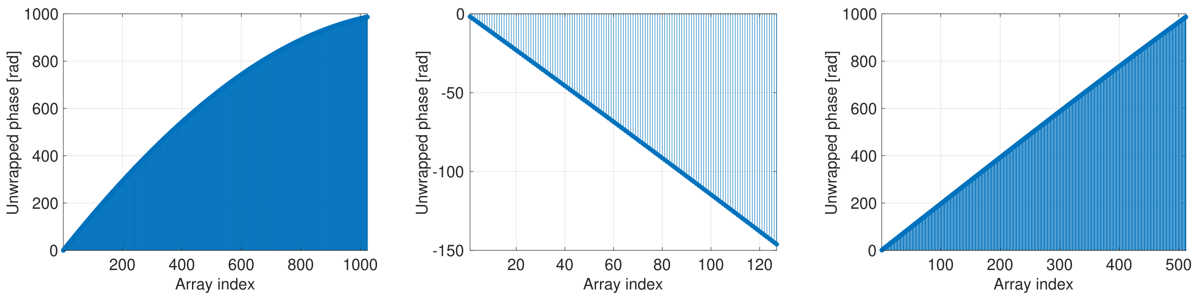

(a) Original channel (size: 1024) (b) CPD channel #1 (size: 128) (c) CPD channel #2 (size: 512)

FIGURE 4. **Unwrapped phase of each channels ($d = 15$ meters, $\theta = \pi/3$ radian, $\lambda = 0.0125$ meters, and $N = 1024$).**

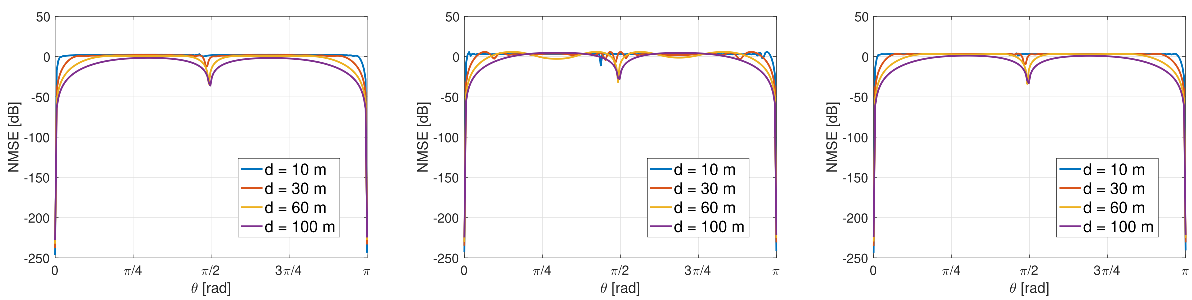

(a) Original channel (size: 1024) (b) CPD channel #1 (size: 128) (c) CPD-channel #2 (size: 512)

FIGURE 5. **Second-order Taylor approximation error of channel ($\lambda = 0.0125$ meters and $N = 1024$).**

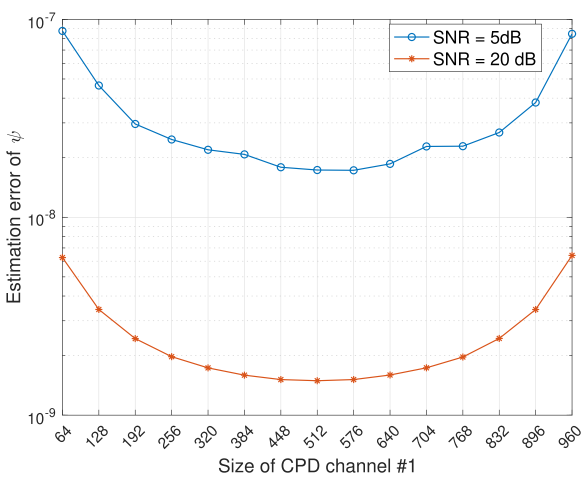

FIGURE 6. **Performance of ψ estimation according to size of CPD channel #1 ($N = 1024$).**

Algorithm 2 CPD-Based User Localization With Noisy Samples

1: [*CPD-based representation phase*].
2: Measure N-sized noisy channel $\mathbf{y}$ and determine index spacing m.
3: Design $(N - m)$-sized CPD channel #1, i.e., $\mathbf{q}(\mathbf{y}; m)$, based on (8).
4: Design $N/2$-sized CPD channel #2, i.e., $\mathbf{p}(\mathbf{y})$, based on (10).
5: Obtain denoised channels $\tilde{\mathbf{q}}(\mathbf{y}; m)$ and $\tilde{\mathbf{p}}(\mathbf{y})$ based on (15), (16) and (17).
6: [*User localization phase*].
7: Perform Steps 6 and 7 of Algorithm 1 after substituting $\tilde{\mathbf{q}}(\mathbf{y}; m)$ and $\tilde{\mathbf{p}}(\mathbf{y})$ for $\mathbf{q}(\mathbf{y}; m)$ and $\mathbf{p}(\mathbf{y})$, respectively.

5) ACCURACY OF THE SECOND-ORDER TAYLOR APPROXIMATION

The proposed method begins by modeling the wavefront using a second-order polynomial representation, commonly referred to as the Fresnel approximation. This approach captures the regional curvature of the wavefront, providing the accurate representation and computational simplicity. While the second-order approximation effectively represents the dominant characteristics of the wavefront, the approximation error term arises from the contributions of higher-order components. This error, as described by the residual terms in Taylor expansions, depends on the user location relative to the wavefront. Variations in the user's location influence the magnitude of higher-order derivatives, thereby introducing a dependency in the approximation accuracy. Therefore, understanding this dependency is crucial for ensuring the robust performance of the proposed method across diverse user locations.

G. PROPOSED METHOD WITH NOISY SAMPLES

In this subsection, we present practical methods for mitigating error in noisy environments. Let us define the noisy channel $\mathbf{y}$ as follows:

$$\mathbf{y} = \mathbf{h} + \mathbf{w}, \tag{14}$$

where $\mathbf{w}$ is the additive white Gaussian noise (AWGN).

First, let us take a closer look at the noiseless environments, i.e., $\mathbf{w}[n] = 0$ for all n. In this case, CPD channels #1 and #2, i.e., $\mathbf{q}(\mathbf{y}; m)$ and $\mathbf{p}(\mathbf{y})$, have an approximately linear phase characteristic as we discussed earlier. In what follows, we describe the denoising procedure by taking $\mathbf{q}(\mathbf{y})$ as the reference CPD channel. Next, the Hankelized matrix $\mathbf{Q} \in \mathbb{C}^{K_1 \times K_2}$ is defined as follows:

$$\mathbf{Q}[i, j] = \mathbf{q}(\mathbf{y}; m)[i + j - 1], \quad \forall i, j \in \{1, 2, \cdots\}, \tag{15}$$

where $K_1 + K_2 = N - m + 1$ and $K_2 = K_1 + 1$. In the noiseless environments and assumption of Fresnel approximation, since $\mathbf{q}(\mathbf{y}; m)$ exhibits a linear phase structure, it can be represented as a single complex exponential sequence. Therefore, the rank of Hankelized matrix $\mathbf{Q}$ is 1, since all rows (and columns) are linearly dependent.

However, due to the noise and approximation error, this rank-1 property is not satisfied, leading to an increase in rank. Therefore, by approximating $\mathbf{Q}$ with a rank-1 matrix using K-singular value decomposition (SVD) [25] for using the largest singular value and its corresponding vectors, we can reduce the noise contribution and retain the dominant signal structure, which can be represented as follows:

$$\tilde{\mathbf{Q}} = \sigma_1 \mathbf{u}_1 \mathbf{v}_1^H, \tag{16}$$

where σ_1 denotes the largest singular value, $\mathbf{u}_1$ and $\mathbf{v}_1$ denote the corresponding left and right singular vectors, respectively. Lastly, the denoised CPD channel can be reconstructed as follows:

$$\tilde{\mathbf{q}}(\mathbf{y}; m)[n] = \frac{1}{u} \sum_{i,j} \tilde{\mathbf{Q}}[i, j], \ s.t. \ i + j - 1 = n, \tag{17}$$

where $u = n$ if $n < K_1$, and $u = N + 1 - n - m$ otherwise, for all $n \in \{1, \cdots, N - m\}$. The same procedure can be applied to the Hankelized matrix $\mathbf{P}$ corresponding to CPD channel #2, i.e., $\mathbf{p}(\mathbf{y})$. Finally, we can extract θ and d using $\tilde{\mathbf{q}}(\mathbf{y}; m)$ and $\tilde{\mathbf{p}}(\mathbf{y})$. Algorithm 2 summarizes the process of localization with noisy samples. Note that the proposed methods evaluated in the simulation section all incorporate the denoising procedure.

TABLE 1. Default configuration in the experiments.

Number of simulations	20000
Array size of the BS (N)	1024
Index spacing size of CPD channel #1 (m)	512
Angle between the BS and the user (θ)	$\mathcal{U}(0, \pi)$ [rad.]
Distance between the BS and the user (d)	$\mathcal{U}(10, 100)$ [meter]
Wavelength (λ)	0.0125 [meter]
Antenna spacing (Δ_s)	0.00625 [meter]

Fig. 7 demonstrates the denoising performance of K-SVD. It shows the denoising performance versus SNR, demonstrating that the K-SVD-based denoising method consistently achieves superior performance across different SNR levels.

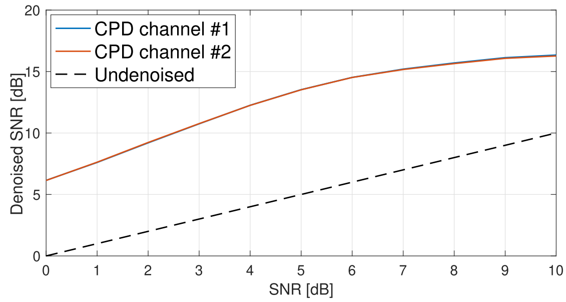

FIGURE 7. Performance of K-SVD-based denoising (Default parameter setting are summarized in Table 1).

As discussed in this section, denoising is first addressed at the signal level within the proposed linear-algebraic framework; nevertheless, neural network (NN)-based techniques may serve as powerful complementary mechanisms that can be incorporated as a post-processing stage to further improve denoising performance. Since acquiring reliable ground-truth labels at the signal-sample level is practically challenging, directly applying NN-based denoising at the user-location level appears to be a more effective and feasible strategy. The corresponding post-processing mechanism is described in the Appendix.

In the following section (i.e., simulation results), the proposed method refers to the version that performs only linear-algebraic signal denoising, excluding the NN-based post-processing (except for Table 2), in order to ensure a fair comparison with other Baselines.

IV. SIMULATION RESULTS

In this section, we numerically evaluate the performance of the proposed method for user localization. The parameter settings for experiments are summarized in Table 1. To assess the performance of the proposed method, two distinct approaches are considered for comparison. The first set of baselines is based on sub-array-based methods [20], including Baseline 1 (half-partitioned) and Baseline 2 (quarter-partitioned). The second set of baselines is based on a polar-dictionary-equipped matching-pursuit-based method [18], comprising Baseline 3 (line-search) and Baseline 4 (brute-force). The spatial frequency estimation within the proposed method is conducted in accordance with [26].

Fig. 8a shows the user localization performance of algorithms as a function of array size. The proposed method demonstrates superior performance across array sizes compared to the baseline approaches. However, as the array size becomes extremely large, the performance of the proposed method tends to degrade. The decline can be attributed to the growing approximation error between the actual channel model and the second-order Taylor approximation, which becomes increasingly significant as the array size expands.

As shown in Fig. 8b, the proposed method demonstrates superior performance across a diverse SNR regime. Under

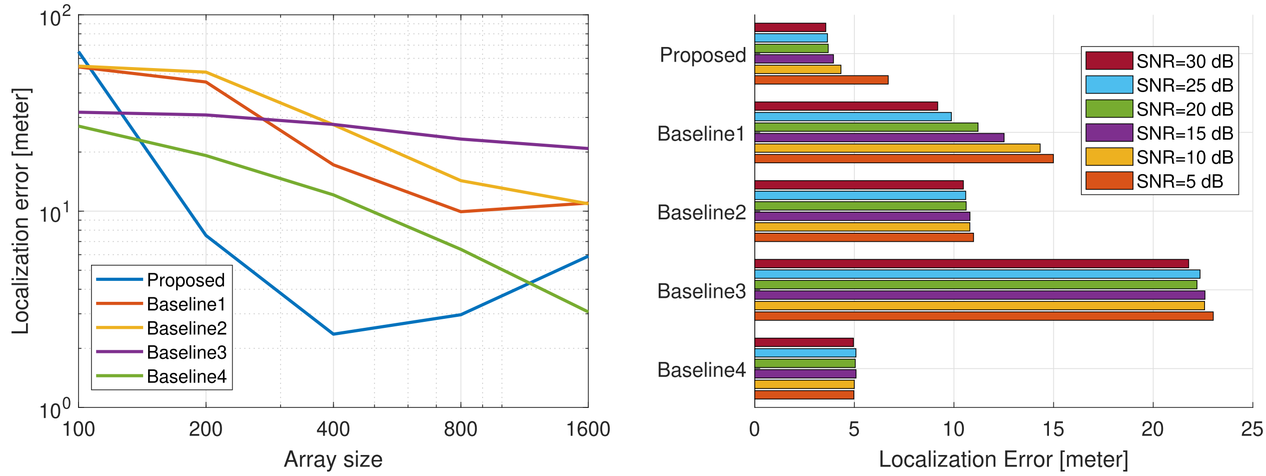

(a) According to array size (SNR: 20 dB)

(b) According to SNR (N: 1024)

FIGURE 8. **Performance of user localization.**

TABLE 2. **Performance of user localization in meters according to SNR (N: 1024).**

Method \ SNR	5 dB	10 dB	15 dB	20 dB	25 dB	30 dB
Proposed (w/o NN post-processing)	7.57	4.64	3.90	3.74	3.62	3.55
Proposed (w/ NN post-processing)	6.77	3.79	3.67	3.50	3.43	3.43

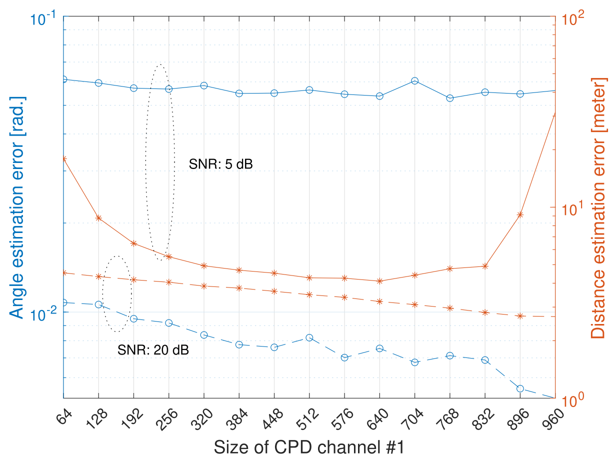

FIGURE 9. **Performance of joint angle-and-distance estimation according to size of CPD channel #1 (N = 1024).**

the low SNR condition, Baseline 4, which performs a brute-force search using the polar dictionary, achieves the best performance. While the proposed method exhibits limitations under the low SNR condition, it achieves superior user localization performance after the SNR exceeds 5 dB. Considering its low computational complexity, the proposed method can be regarded as a highly effective approach.

Fig. 9 shows the performance of angle and distance estimation when varying the size of CPD channel #1 (i.e., $N - m$). When the SNR is 20 dB, the increment of the size of CPD channel #1 leads to better performance in terms of θ and d. This comes from accurate estimation of $m\phi$ in (9) and (12). In contrast, at an SNR of 5 dB, the performance of distance estimation shows a concave-shaped curve in terms of the selection of m. This is related to the ability to estimate $m\psi$ itself (determined by the size of $N - m$) and the performance variation caused by dividing the estimated value by m to extract the core information ψ. In other words, $m\psi$ needs to span a wider normalized angular range to ensure greater robustness under the same level of error factors, which necessitates a sufficiently large m. In summary, when a high SNR is ensured, sufficient resolution for $m\psi$ estimation can be achieved, making it advantageous to design with a smaller m. Conversely, in low-SNR environments, it is beneficial to set the value of m, considering the trade-off relationship associated with its selection.

Further, Table 2 demonstrates the performance improvement of the proposed method itself achieved by using the NN-assisted localization method described in the Appendix. In the simulations, the network width is set to 24, the network depth to 2, the activation function to the sigmoid function, and the number of training samples to 5000. Across all SNR levels, the proposed method with denoising and NN consistently outperforms the version without NN. The performance gain is particularly noticeable in the low SNR regime, e.g., 5-10 dB, where the NN effectively compensates for residual estimation errors.

V. CONCLUSION

This paper presents a novel channel representation technique, termed CPD, designed to enhance user localization accuracy in near-field LoS environments. By employing a second-order Taylor approximation for phase linearization, we derived a model that seamlessly captures the quadratic phase variations inherent to near-field channels, transforming them into a simplified linear representation. Simulation results validate that this pairwise-division-based method achieves superior localization accuracy compared to the conventional approaches. While the proposed CPD model offers notable advantages, such as wide versatility and low computational complexity, certain practical challenges must be rigorously addressed, which are SNR degradation, the effects of mixed LoS and NLoS propagation, and the accuracy of the second-order Taylor approximation. Notwithstanding these considerations, the proposed method constitutes a promising framework for near-field localization, with considerable potential for extension to more complex channel conditions.

APPENDIX
NEURAL NETWORK-ASSISTED POST-PROCESSOR FOR THE CPD-BASED SCHEME

We present the neural network (NN)-based user localization method for noisy environment in order to further enhance the proposed method. In a nutshell, the input of NNs is estimated angle $\tilde{\theta}$ and distance $\tilde{d}$ after going through denoising procedure, and the output is set by the original angle θ and distance d, respectively. Now we design the NNs. The optimal estimation function $\mathcal{L}_o^* : \mathbb{R} \mapsto \mathbb{R}$, where $o \in \{\theta, d\}$ can be constructed as follows:

$$\mathcal{L}_o^* = \underset{\mathcal{L}_o}{\operatorname{argmin}} \frac{1}{N'} \sum_{i=1}^{N'} ||\tilde{o}^{(i)} - o^{(i)}||_2^2, \tag{18}$$

where N' and i are the number and the index of the training dataset, respectively. Note that $\mathcal{L}_\theta^*$ and $\mathcal{L}_d^*$ are angle estimator and distance estimator, respectively. We choose the scaled conjugate gradient algorithm as the optimizer that update rule for the NN models. Finally, the estimated angle and distance based on the NN approach, denoted by $\hat{\theta}$ and $\hat{d}$, respectively, can be represented as follows:

$$\hat{\theta} = \mathcal{L}_\theta^*(\tilde{\theta}) \text{ and } \hat{d} = \mathcal{L}_d^*(\tilde{d}). \tag{19}$$

REFERENCES

[1] M. Cui, Z. Wu, Y. Lu, X. Wei, and L. Dai, "Near-field MIMO communications for 6G: Fundamentals, challenges, potentials, and future directions," *IEEE Commun. Mag.*, vol. 61, no. 1, pp. 40–46, Jan. 2023.

[2] T. S. Rappaport, Y. Xing, O. Kanhere, S. Ju, A. Madanayake, S. Mandal, A. Alkhateeb, and G. C. Trichopoulos, "Wireless communications and applications above 100 GHz: Opportunities and challenges for 6G and beyond," *IEEE Access*, vol. 7, pp. 78729–78757, 2019.

[3] H. Do, S. Cho, J. Park, H.-J. Song, N. Lee, and A. Lozano, "Terahertz line-of-sight MIMO communication: Theory and practical challenges," *IEEE Commun. Mag.*, vol. 59, no. 3, pp. 104–109, Mar. 2021.

[4] H. Do, N. Lee, and A. Lozano, "Parabolic wavefront model for line-of-sight MIMO channels," *IEEE Trans. Wireless Commun.*, vol. 22, no. 11, pp. 7620–7634, Nov. 2023.

[5] H. Zhang, N. Shlezinger, F. Guidi, D. Dardari, and Y. C. Eldar, "6G wireless communications: From far-field beam steering to near-field beam focusing," *IEEE Commun. Mag.*, vol. 61, no. 4, pp. 72–77, Apr. 2023.

[6] J.-H. Kim, D.-H. Kim, M. Ozger, and W.-H. Lee, "An NN-aided near-and-far-field classifier via channel hankelization in XL-MIMO systems," *IEEE Access*, vol. 12, pp. 41934–41941, 2024.

[7] Y. Liu, J. Xu, Z. Wang, X. Mu, and L. Hanzo, "Near-field communications: What will be different?" *IEEE Wireless Commun.*, vol. 32, no. 2, pp. 262–270, Apr. 2025.

[8] H. Zhang, N. Shlezinger, F. Guidi, D. Dardari, M. F. Imani, and Y. C. Eldar, "Beam focusing for near-field multiuser MIMO communications," *IEEE Trans. Wireless Commun.*, vol. 21, no. 9, pp. 7476–7490, Sep. 2022.

[9] X. Li, Z. Dong, Y. Zeng, S. Jin, and R. Zhang, "Multi-user modular XL-MIMO communications: Near-field beam focusing pattern and user grouping," *IEEE Trans. Wireless Commun.*, vol. 23, no. 10, pp. 13766–13781, Oct. 2024.

[10] Y. Zhang and A. Alkhateeb, "Deep learning of near field beam focusing in terahertz wideband massive MIMO systems," *IEEE Wireless Commun. Lett.*, vol. 12, no. 3, pp. 535–539, Mar. 2023.

[11] S. Yang, H. Chen, W. Liu, X.-P. Zhang, and C. Yuen, "Near-field channel estimation and localization: Recent developments, cooperative integration, and future directions," *IEEE Signal Process. Mag.*, vol. 42, no. 1, pp. 60–73, Jan. 2025.

[12] Z. Lu, Y. Han, S. Jin, and M. Matthaiou, "Near-field localization and channel reconstruction for ELAA systems," *IEEE Trans. Wireless Commun.*, vol. 23, no. 7, pp. 6938–6953, Jul. 2024.

[13] H. Lei, J. Zhang, Z. Wang, B. Ai, and E. Bjornson, "Near-field user localization and channel estimation for XL-MIMO systems: Fundamentals, recent advances, and outlooks," *IEEE Wireless Commun.*, vol. 32, no. 4, pp. 190–198, Aug. 2025.

[14] J. Cong, C. You, J. Li, L. Chen, B. Zheng, Y. Liu, W. Wu, Y. Gong, S. Jin, and R. Zhang, "Near-field integrated sensing and communication: Opportunities and challenges," *IEEE Wireless Commun.*, vol. 31, no. 6, pp. 162–169, Dec. 2024.

[15] S. Eslami, B. Gouda, and A. Tölli, "Near-field MIMO channel reconstruction via limited geometry feedback," in *Proc. ICASSP - IEEE Int. Conf. Acoust., Speech Signal Process. (ICASSP)*, Apr. 2024, pp. 9256–9260.

[16] N. J. Myers, J. Kaleva, A. Tölli, and R. W. Heath, "Message passing-based link configuration in short range millimeter wave systems," *IEEE Trans. Commun.*, vol. 68, no. 6, pp. 3465–3479, Jun. 2020.

[17] D. Gürgünoğlu, A. Kosasih, P. Ramezani, Ö. T. Demir, E. Björnson, and G. Fodor, "Performance analysis of a 2D-MUSIC algorithm for parametric near-field channel estimation," *IEEE Wireless Commun. Lett.*, vol. 14, no. 5, pp. 1496–1500, May 2025.

[18] M. Cui and L. Dai, "Channel estimation for extremely large-scale MIMO: Far-field or near-field?" *IEEE Trans. Commun.*, vol. 70, no. 4, pp. 2663–2677, Apr. 2022.

[19] J. Li, Q. Chen, and F. Xi, "A blind super-resolution method for near-field channel estimation with angle-range recovery," in *Proc. IEEE Int. Conf. Acoust., Speech Signal Process. (ICASSP)*, Apr. 2025, pp. 1–5.

[20] H.-T. Chou, M. R. Pino, P. Nepa, and C.-Y. Liu, "Near-field focused subarrays in a multi-panel configuration," *IEEE Access*, vol. 7, pp. 143097–143108, 2019.

[21] Y. Zheng, M. Zhang, B. Teng, and X. Yuan, "Scalable near-field localization based on array partitioning and angle-of-arrival fusion," in *Proc. IEEE Int. Conf. Commun.*, Jun. 2024, pp. 4415–4420.

[22] S. Shin, J. Moon, S. Kim, and B. Shim, "Subarray-based near-field beam training for 6G terahertz communications," in *Proc. IEEE Int. Conf. Commun.*, Jun. 2024, pp. 3189–3194.

[23] E. Björnson, C.-B. Chae, R. W. Heath, T. L. Marzetta, A. Mezghani, L. Sanguinetti, F. Rusek, M. R. Castellanos, D. Jun, and Ö. T. Demir, "Towards 6G MIMO: Massive spatial multiplexing, dense arrays, and interplay between electromagnetics and processing," 2024, *arXiv:2401.02844*.

[24] A. Kosasih, Ö. T. Demir, N. Kolomvakis, and E. Björnson, "Spatial frequencies and degrees of freedom: Their roles in near-field communications," 2024, *arXiv:2407.07448*.

[25] K. Shin, J. K. Hammond, and P. R. White, "Iterative SVD method for noise reduction of low-dimensional chaotic time series," *Mech. Syst. Signal Process.*, vol. 13, no. 1, pp. 115–124, Jan. 1999.

[26] W.-H. Lee, J.-H. Lee, and K. W. Sung, "Geometric sequence decomposition with k-simplexes transform," *IEEE Trans. Commun.*, vol. 69, no. 1, pp. 94–107, Jan. 2021.

WOONG-HEE LEE (Member, IEEE) received the B.S. degree in electrical engineering from Korea Advanced Institute of Science and Technology (KAIST), Daejeon, South Korea, in 2009, and the Ph.D. degree in electrical engineering from Seoul National University, Seoul, South Korea, in 2017. From 2017 to 2019, he was an Experienced Researcher with the Advanced Standard Research and Development Laboratories, LG Electronics Inc., Seoul. From 2019 to 2020, he was a Postdoctoral Researcher with the Department of Communication Systems, KTH Royal Institute of Technology, Stockholm, Sweden. He was an Experienced Researcher with Ericsson Research, Stockholm. From 2021 to 2024, he was an Assistant Professor with the Department of Control and Instrumentation Engineering, Korea University, Sejong-si, Republic of Korea. Since March 2024, he has been an Assistant Professor with the Division of Electronics and Electrical Engineering, Dongguk University, Seoul. His research interests include signal processing, machine learning, and game theory in wireless communications.

DONG-HWAN KIM received the B.S. degree in electro-mechanical engineering from Korea University, Sejong, Republic of Korea, in 2025. He is currently pursuing the M.S. degree with the Division of Electronics and Electrical Engineering, Dongguk University, Seoul, Republic of Korea. His research interests include signal processing and machine learning in wireless communications, with additional academic interests in information theory.

HYUNDUK KANG received the B.Eng. degree in electronics engineering from Dong-A University, Busan, South Korea, in 1997, and the M.S. and Ph.D. degrees in information and communication engineering from Gwangju Institute of Science and Technology (GIST), Gwangju, South Korea, in 1999 and 2006, respectively. In 2006, he joined the Electronics and Telecommunications Research Institute (ETRI) as a Senior Member of the Engineering Staff in the Radio Technology Research Department. He is currently a Principal Researcher with the Radio Resource Research Section, Radio Research Division. He has been involved in several projects related to radio resource management, performance evaluation of cognitive radio systems, and the IEEE 802.19 standardization on wireless coexistence in the TV white space. His research interests include radio resource management, interference analysis, coexistence evaluation, and spectrum engineering in wireless communication systems.

HO-KYUNG SON received the B.S. and M.S. degrees in electronic engineering, and the Ph.D. degree from Kyungpook National University, Daegu, South Korea, in 1997, 1999, and 2013, respectively. From March 1999 to March 2000, she was a Researcher with LG Information and Communication. Since May 2000, she has been with the Electronics and Telecommunications Research Institute (ETRI), Daejeon, South Korea, where she is a Principal Researcher with the Radio Resource Research Section, Radio Research Division. Her research interests include radio resource management, interference analysis between wireless communications, and radio propagation.

JONG-HO LEE (Member, IEEE) received the B.S. degree in electrical engineering, and the M.S. and Ph.D. degrees in electrical engineering and computer science from Seoul National University, Seoul, South Korea, in 1999, 2001, and 2006, respectively. From 2006 to 2008, he was a Senior Engineer with Samsung Electronics, Suwon, South Korea. From 2008 to 2009, he was a Postdoctoral Researcher with Georgia Institute of Technology, Atlanta, GA, USA. From 2009 to 2012, he was an Assistant Professor with the Division of Electrical, Electronic, and Control Engineering, Kongju National University, Cheonan, South Korea. From 2012 to 2018, he was an Associate Professor with the Department of Electronic Engineering, Gachon University, Seongnam, South Korea. Since 2018, he has been a Faculty Member with the School of Electronic Engineering, Soongsil University, Seoul. His research interests include wireless communication systems and signal processing for communication, with an emphasis on multiple-antenna techniques, multi-hop relay networks, physical-layer security, and full-duplex wireless communications.

NAMYOON LEE (Senior Member, IEEE) received the Ph.D. degree from The University of Texas at Austin, in 2014.

He was with the Communications and Network Research Group, Samsung Advanced Institute of Technology, South Korea, from 2008 to 2011, and later worked with the Wireless Communications Research, Intel Laboratories, Santa Clara, CA, USA, from 2015 to 2016. He has been a Professor with Pohang University of Science and Technology (POSTECH), since 2016. His research interests include communications theory, with a focus on advanced multi-antenna communications, channel coding technologies, and future wireless systems. He has received several prestigious awards, including the 2016 IEEE ComSoc Asia-Pacific Outstanding Young Researcher Award, the 2020 IEEE Best Young Professional Award (Outstanding Nominee), the 2021 IEEE-IEIE Joint Award for Young Engineer and Scientist, and the 2021 KICS Haedong Young Engineering Researcher Award. He has actively contributed to IEEE journals and conferences, serving as an Associate Editor for IEEE Communications Letters, from 2018 to 2020, and IEEE Transactions on Vehicular Technology, from 2021 to 2023. He was also a Guest Editor of *IEEE Communications Magazine* in the Special Issue on Near-Field MIMO Technologies Toward 6G. Since 2021, he has been an Associate Editor for IEEE Transactions on Wireless Communications and IEEE Transactions on Communications.